Eur. Phys. J. B **47**, 295–303 (2005)
DOI: 10.1140/epjb/e2005-00324-y

THE EUROPEAN PHYSICAL JOURNAL B

# Spin-flip mesoscopic transport through a quantum dot coupled to carbon nanotube terminals

H.-K. Zhao[1,2,a] and L.-N. Zhao[2]

[1] CCAST (World Laboratory), P.O. Box 8730, Beijing 100080, P.R. China
[2] Department of Physics, Beijing Institute of Technology, Beijing 100081, P.R. China

Received 8 April 2005 / Received in final form 30 May 2005
Published online 11 October 2005 – 

**Abstract.** We investigate mesoscopic transport through a system that consists of a central quantum dot (QD) and two single-wall carbon nanotube (SWCN) leads in the presence of a rotating magnetic field. The spin-flip effect is induced by the rotating magnetic field, and the tunnelling current is sensitively related to the spin-flip effect. We present the calculations of charge and spin current components to show the intimate relations to the SWCN leads. Zeeman effect is important when the applied magnetic field is strong enough. The current characteristics are quite different when the source-drain bias is zero ($eV = 0$) and nonzero ($eV \neq 0$). The asymmetric peak and valley of spin current versus gate voltage exhibit Fano resonance. Multi-resonant peaks of spin current versus photon energy $\hbar\omega$ reflect the structure of CN quantum wires, as well as the resonant photon absorption and emission effect. The matching-mismatching of channels in the CN leads and QD results in novel spin current structure by tuning the frequency.

**PACS.** 73.40.-c Electronic transport in interface structures – 73.63.Fg Nanotubes – 73.61.Wp Fullerenes and related materials 73.22.-f Electronic structure of nanoscale materials: clusters, nanoparticles, nanotubes, and nanocrystals

## 1 Introduction

Charge and spin are two degrees of freedom for describing the nature of individual electrons. Usually the effect of spin is very small in non-magnetic materials, and it can be neglected in the absence of magnetic field. However, the spin of an electron is responded to an applied magnetic field sensitively. The investigation on the affection and effect of spin degree in materials is still in process, and it is unmatured comparing with the study of charge degree of freedom both for the fundamental and applied physics. The motivation of employing the specific effects of spin in materials naturally makes scientists to contrive novel nano-devices for potential applications [1]. Datta and Das have made the pioneering contribution to the exploration of spin-dependent semiconducting nano-device. They have proposed an electron wave analog of electro-optic light modulator. In reference [2], the current modulation in the proposed structure arises from the spin precession due to spin-orbit coupling in narrow-gap semiconductor. The theoretical work of efficient spin filter has been discussed based on a quantum dot (QD) in the Coulomb blockade regime weakly coupled to current leads [3]. The Rashba term takes effect in a nonmagnetic resonant tunnelling diode [4]. Such spin filter and spin memory systems could be chosen as functional devices of quantum computer. Several theoretical spin battery models, or spin generators, have been contrived for generating spins current, for instance, the precessing ferromagnetic injection [5], the double QD under a microwave radiation [6,7], and a spin field effect transistor (SFET) applied with a rotating magnetic field [8]. Therefore a very prosperous frontier of investigation known as spintronics is developing correspondingly. The dissipatedness spin transport [9], quantized spin conductance in insulating system provide some examples of spintronics [10]. The experiments on the control and manipulation of spin make it possible for the fabrication of spin electronic devices [11]. Recently, one of the authors et al. have made some contributions to this field: (1) by considering mesoscopic spin transport through a quantum dot responded by a rotating and an oscillating magnetic fields; (2) the spin tunnelling through a coupled toroidal carbon nanotube system in the presence of a rotating magnetic field and an Aharonov-Bohm magnetic flux [12].

On the other hand, the single-wall carbon nanotubes (SWCNs) are ideal materials and samples for investigation because of their unique electronic features. Examples of such prosperous investigations on this field are associated with the metal-semiconductor transition [13], the long spin coherent length [14], the Schottky barrier in metal-semiconductor junction [15], the features of diode [16], and field effect transistor [17]. SWCNs provide natural materials of quasi-one-dimensional quantum wire for investigation, and they contain rich physical band structure for verifying and revealing physical characteristics in laboratory.

[a] e-mail: zhaohonk@yahoo.com

The combination of nano-technology based on spintronics and CNs is thought to be extremely promising for future electronic device innovations [18]. All these make the carbon nanotubes (CNs) to be prospective materials for nano-devices in future application. In this paper we study the spin transport, as well as the charge transport through a coupled system which consists of a central quantum dot and two CN leads. The QD is controlled by a metallic gate capacitively coupled to the QD. The source and drain are biased by a voltage $V$ in general to induce charge current. We consider the situation that the QD is applied by a rotating magnetic field, and the spin current is generated. This rotating field induces spin-flip effect, which can be employed as a spin generator [8]. Here we focus our attention to the circumstance that the mesoscopic spin and charge transport are controlled by source-drain bias with the influences of CN leads. The density of states (DOS) of CNs present specific effect to the resultant electronic properties due to the special electronic structures. The usual wide-band limit method of calculation is invalid.

We arrange the remainder of the paper as follows. Section 2 presents the formalism and derivation of tunnelling current by employing the nonequilibrium Green's function technique. The charge and spin current formulas are given there. Section 3 is devoted to the numerical calculations and discussions of the obtained results. There we make some comparisons with the system coupled with normal leads. Brief conclusion and remarks are given in the final section.

## 2 Model and formalism

We consider the system which is consisted of a QD coupled to one left and one right CN leads. The QD is relatively large, and the intra-dot electron interaction is neglected. The size of QD is about 10 nm in three dimensions. We assume that the right and left CN leads are located in $\mathbf{e}_y$ direction, and the $\mathbf{e}_z$ direction is perpendicular to the CN leads. A rotating magnetic field with angular frequency $\omega$ is applied to the QD, and it is screened in order not to affect the leads. The magnetic field rotates around the z-axis with the tilt angle $\theta$, i.e., $\mathbf{B}(t) = B_0[\sin\theta\cos(\omega t)\mathbf{e}_x + \sin\theta\sin(\omega t)\mathbf{e}_y + \cos\theta\mathbf{e}_z]$, where $B_0$ is the constant field strength. Spin-flip effect is induced by this rotating field, and it is the major source of spin current. The Hamiltonian of our system is composed of the three subsections and the tunnelling term as

$$\begin{aligned} H = &\sum_{\delta\gamma k\sigma} \varepsilon_{\delta\gamma,k\sigma} c^\dagger_{\delta\gamma,k\sigma} c_{\delta\gamma,k\sigma} + \sum_{\ell\sigma} \tilde{E}_{\ell\sigma}(\theta) d^\dagger_{\ell\sigma} d_{\ell\sigma} \\ &+\xi \sum_{\ell} \left[\exp(-i\omega t) d^\dagger_{\ell\uparrow} d_{\ell\downarrow} + \exp(i\omega t) d^\dagger_{\ell\downarrow} d_{\ell\uparrow}\right] \\ &+ \sum_{\delta\gamma k\ell\sigma} \left[R_\gamma c^\dagger_{\delta\gamma,k\sigma} d_{\ell\sigma} + \text{H.c.}\right], \end{aligned} \tag{1}$$

with $\xi = \mu_B B_0 \sin\theta$, $\tilde{E}_{\ell\sigma}(\theta) = E_\ell + \sigma\mu_B B_0 \cos\theta$, and $\mu_B$ being the Bohr magneton. In the Hamiltonian, the operators $c^\dagger_{\delta\gamma,k\sigma}(c_{\delta\gamma,k\sigma})$, and $d^\dagger_{\ell\sigma}(d_{\ell\sigma})$ are the creation (annihilation) operators of electron in the two CN leads and the central QD, respectively. The spin subscript $\sigma$ takes the value $\sigma = \pm 1$, which denotes the situation for spin-up $\uparrow$, and spin-down $\downarrow$. We use the tight binding model to describe the electronic properties of the SWCN leads where the Coulomb interaction is neglected [18,19]. Although this is simple compared with the first principle approach [20] and Luttinger model [21,22], it makes us to understand the main physical feature of mesoscopic transport problems [23]. The second and third terms stand for the Hamiltonian of QD subjected to the external rotating magnetic field. $E_\ell = E^0_\ell - eV_g$ indicates that the electron levels of QD are controlled by the gate voltage $V_g$, where $E^0_\ell$ is the energy level of QD in the absence of external field. $R_\gamma$ is the interaction strength of electrons between the $\gamma$th lead and the central QD. The electronic structures of CN leads make important contributions to the output characteristics. The CN leads act as quantum wires, since the quasi-one-dimensional terminals possess special energy structure. Two kinds of CNs with highly symmetric structure are armchair $(n,\, n)$ CN and zigzag $(n,\, 0)$ CN. In the absence of magnetic flux, the armchair $(n,\, n)$ CN is metallic. For the zigzag $(n,\, 0)$ CN in the absence of magnetic flux, it is metallic as $n = 3\nu$, while it is semiconducting with narrow energy gap as $n = 3\nu \pm 1$, where $\nu$ is an integer. The energy of a CN lead is quantized in the transverse direction, while it is not restricted in the longitudinal direction. The energies of armchair and zigzag CN leads in the tight-binding approximation are given by [24]

$$\begin{aligned} \varepsilon_{\delta\gamma,k\sigma} = \delta\gamma_0 \Bigg\{1 + 4\cos\left(\frac{ak_y}{2}\right) \\ \times \cos\left(\frac{q\pi}{n}\right) + 4\cos^2\left(\frac{ak_y}{2}\right)\Bigg\}^{\frac{1}{2}}, \end{aligned}$$

$$\begin{aligned} \varepsilon_{\delta\gamma,k\sigma} = \delta\gamma_0 \Bigg\{1 + 4\cos\left(\frac{q\pi}{n}\right) \\ \times \cos\left(\frac{\sqrt{3}ak_y}{2}\right) + 4\cos^2\left(\frac{q\pi}{n}\right)\Bigg\}^{\frac{1}{2}}, \end{aligned}$$

where $q = 1, 2, \ldots, 2n$, $\delta = \pm$, and $\gamma_0 = 3.033$ eV. Here $a = b \times 3^{1/2}$, and $b = 1.44$ Å is the C–C bond length of CNs known to be slightly larger than that of graphite. We have investigated the mesoscopic transport through similar systems in the absence of rotating field, but some novel features are revealed in the current characteristics under microwave fields [25,26].

The tunnelling current depending on spin components in the $\gamma$th lead can be derived by employing the Heisenberg equation and continuity equation

$$\begin{aligned} J^\gamma_{\sigma'\sigma}(t) = \frac{i}{\hbar} \sum_{\delta k\ell} \Big[R_\gamma \langle c^\dagger_{\delta\gamma,k\sigma'}(t) d_{\ell\sigma}(t)\rangle \\ - R^*_\gamma \langle d^\dagger_{\ell\sigma'}(t) c_{\delta\gamma,k\sigma}(t)\rangle\Big]. \end{aligned} \tag{2}$$

This current formula describes the injection of electrons with the spin index $\sigma$ from the $\gamma$th lead to QD. As the electrons are injected into QD, the rotating magnetic field and local electrons interact with the incident electrons, and the tunnelling current is asymmetric due to spin-flip effect in the scattering regime. The spin current and charge current are composed of spin-up and spin-down current components. The charge current is determined by $I_c = e\sum_\sigma J^L_{\sigma\sigma} = e(J^L_{\uparrow\uparrow} + J^L_{\downarrow\downarrow})$ and the $\mathbf{s}_z$ component spin current is determined by $I_s = \hbar(J^L_{\downarrow\downarrow} - J^L_{\uparrow\uparrow})/2$. Usually, in the absence of magnetic field, the current components are equal even if the system is spin non-degenerate, and the spin current is zero. However, as the rotating magnetic field is applied, this system can be taken as a spin generator, but the spin current is not conserved.

In order to derive the tunnelling current, we define the Green's function $G^X_{\ell\sigma,\ell'\sigma'}(t,t')$ of the coupled QD system as $G^X_{\ell\sigma,\ell'\sigma'}(t,t') = \langle\langle d_{\ell\sigma}(t), d^\dagger_{\ell'\sigma'}(t')\rangle\rangle^X$, where $X \in \{r, a, <\}$ [27–29]. Employing the decoupling procedure proposed by Jauho et al. [27], the tunnelling current can be determined by the Green's functions of QD as

$$J^\gamma_{\sigma'\sigma}(t) = \frac{2}{h}\mathrm{Re}\sum_\ell \int \frac{d\epsilon_1 d\epsilon_2}{2\pi\hbar}\Gamma_{\gamma\sigma}(\epsilon_2)e^{-\frac{i}{\hbar}(\epsilon_1-\epsilon_2)t} \times \left[G^r_{\ell\sigma,\ell\sigma'}(\epsilon_1,\epsilon_2)f_\gamma(\epsilon_2) + \frac{1}{2}G^<_{\ell\sigma,\ell\sigma'}(\epsilon_1,\epsilon_2)\right]. \quad (3)$$

The Fermi distribution function of the $\gamma$th lead is defined as $f_\gamma(\epsilon) = 1/\{\exp[(\epsilon-\mu_\gamma)/K_BT]+1\}$. $\Gamma_{\gamma\sigma}(\epsilon)$ is the line-width function of the $\gamma$th lead defined by $\Gamma_{\gamma\sigma}(\epsilon) = 2\pi \mid R_\gamma \mid^2 \rho_{\gamma\sigma}(\epsilon)$, where $\rho_{\gamma\sigma}(\epsilon)$ is the DOS of corresponding CN lead $\rho_{\gamma\sigma}(\epsilon) = \sum_{k\delta}\delta(\epsilon - \varepsilon_{\delta\gamma,k\sigma})$. The influence of CNs on the mesoscopic transport is contained in the line-width functions through the DOS of CN leads. This means that the central problem is to solve the nonequilibrium Green's functions.

The retarded Green's function of the coupled QD can be derived from the Dyson-like equation

$$G^r_{\ell\sigma,\ell'\sigma'}(t,t') = \xi\int dt_1 e^{-i\sigma\omega t_1}G^{(0)r}_{\ell\sigma,\ell\sigma}(t,t_1)G^r_{\ell\bar\sigma,\ell'\sigma'}(t_1,t') + \sum_{\ell''}\int\int dt_1dt_2 G^{(0)r}_{\ell\sigma,\ell\sigma}(t,t_1)\Sigma^r_\sigma(t_1,t_2) \times G^r_{\ell''\sigma,\ell'\sigma'}(t_2,t') + G^{(0)r}_{\ell\sigma,\ell'\sigma'}(t,t'). \quad (4)$$

In equation (4), we have defined the Green's function of isolated QD as

$$G^{(0)r}_{\ell\sigma,\ell'\sigma'}(t,t') = -\frac{i}{\hbar}\theta(t-t')\exp\left[-\frac{i}{\hbar}\tilde E_{\ell\sigma}(\theta)(t-t')\right]\delta_{\ell\ell'}\delta_{\sigma\sigma'}$$

in the presence of Zeeman field. The total self-energy of coupled CN leads is determined by $\Sigma^{r(a)}_\sigma(t_1,t_2) = \sum_{\delta\gamma k} \mid R_\gamma \mid^2 g^{r(a)}_{\delta\gamma,k\sigma}(t_1,t_2)$, which is given by the Green's function of isolated CN leads $g^{r(a)}_{\delta\gamma,k\sigma}(t_1,t_2) = \mp\frac{i}{\hbar}\theta(\pm t_1 \mp t_2)\exp[-\frac{i}{\hbar}\varepsilon_{\delta\gamma,k\sigma}(t_1-t_2)]$. One can obtain equation (4) by employing the equation of motion, the decoupling procedure, and by expressing it in the integral form. Since the system is perturbed by the rotating magnetic field, the Green's function (4) is dependent on the two times $t, t'$. This indicates that the time reversal symmetry is broken.

Similarly, the Keldysh Green's function can be derived from the integral equation

$$G^<_{\ell\sigma,\ell'\sigma'}(t,t') = \xi\int dt_1 e^{-i\sigma\omega t_1}G^{(0)r}_{\ell\sigma,\ell\sigma}(t,t_1)G^<_{\ell\bar\sigma,\ell'\sigma'}(t_1,t') + \sum_{\ell''}\int\int dt_1dt_2 G^{(0)r}_{\ell\sigma,\ell\sigma}(t,t_1)[\Sigma^r_\sigma(t_1,t_2)G^<_{\ell''\sigma,\ell'\sigma'}(t_2,t') + \Sigma^<_\sigma(t_1,t_2)G^a_{\ell''\sigma,\ell'\sigma'}(t_2,t')]. \quad (5)$$

We have defined the Keldysh self-energy $\Sigma^<_\sigma(t_1,t_2) = \sum_{\delta\gamma k} \mid R_\gamma \mid^2 g^<_{\delta\gamma,k\sigma}(t_1,t_2)$ in equation (5), which is determined by the Keldysh Green's function of CN leads by $g^<_{\delta\gamma,k\sigma}(t_1,t_2) = \frac{i}{\hbar}f(\varepsilon_{\delta\gamma,k\sigma})\exp[-\frac{i}{\hbar}\varepsilon_{\delta\gamma,k\sigma}(t_1-t_2)]$. Equations (4) and (5) contain the spin-flip effect, which is associated with the terms described by the Green's function $G^X_{\ell\bar\sigma,\ell'\sigma'}(t_1,t')$. This signifies that the Green's function $G^X_{\sigma,\sigma}$ is determined by the spin-flip Green's function $G^X_{\sigma,\bar\sigma}$. We are interested in the situation that the magnetic field is strong enough, and the frequency of rotating magnetic field is located in the microwave field regime. This means that the adiabatic approximation is invalid.

We make the Fourier transformation over equation (4) with respect to $t$ and $t'$, and by simple algebraic calculation, we obtain the retarded Green's function of the QD as

$$G^r_{\ell\sigma,\ell'\sigma'}(\epsilon,\epsilon') = 2\pi\hbar G^r_{\ell\sigma,\ell\sigma}(\epsilon)[\delta(\epsilon-\epsilon')\delta_{\ell\ell'}\delta_{\sigma\sigma'} + \xi\tilde G^r_{\ell\bar\sigma}(w_\sigma)\delta(w_\sigma-\epsilon')\delta_{\ell\ell'}\delta_{\bar\sigma\sigma'}], \quad (6)$$

where $w_\sigma = \epsilon + \bar\sigma\hbar\omega$, $\tilde G^r_{\ell\sigma}(\epsilon) = g^r_{\ell\sigma}(\epsilon)/[1 - g^r_{\ell\sigma}(\epsilon)\Sigma^r_\sigma(\epsilon)]$ and $G^r_{\ell\sigma,\ell\sigma}(\epsilon) = \tilde G^r_{\ell\sigma}(\epsilon)/[1-\xi^2\tilde G^r_{\ell\sigma}(\epsilon)\tilde G^r_{\ell\bar\sigma}(\epsilon+\bar\sigma\hbar\omega)]$. The Fourier transformed retarded Green's function of the isolated QD is defined by $g^r_{\ell\sigma}(\epsilon) = 1/[\epsilon - \tilde E_{\ell\sigma}(\theta) + i\eta]$. The total self-energy of leads is given by the summation of self-energy of each CN lead as $\Sigma^r_\sigma(\epsilon) = \sum_{\delta\gamma k} \mid R_\gamma \mid^2 g^r_{\delta\gamma,k\sigma}(\epsilon)$. This self-energy is determined by the Fourier transformed retarded Green's function of isolated CN leads $g^r_{\delta\gamma,k\sigma}(\epsilon) = 1/(\epsilon - \varepsilon_{\delta\gamma,k\sigma} + i\eta)$, $(\eta\to 0)$.

Similarly, by making Fourier transformation over equation (5), direct derivation results in the Keldysh Green's function

$$G^<_{\ell\sigma,\ell'\sigma'}(\epsilon,\epsilon') = 2\pi\hbar|G^r_{\ell\sigma,\ell\sigma}(\epsilon)|^2\{[\xi^2|\tilde G^r_{\ell\bar\sigma}(w_\sigma)|^2\Sigma^<_{\bar\sigma}(w_\sigma) + \Sigma^<_\sigma(\epsilon)]\delta(\epsilon-\epsilon')\delta_{\ell\ell'}\delta_{\sigma\sigma'} + \xi[\frac{|\tilde G^r_{\ell\bar\sigma}(w_\sigma)|^2}{\tilde G^a_{\ell\sigma}(\epsilon)}\Sigma^<_{\bar\sigma}(w_\sigma) + \tilde G^a_{\ell\bar\sigma}(w_\sigma)\Sigma^<_\sigma(\epsilon)]\delta(w_\sigma-\epsilon')\delta_{\ell\ell'}\delta_{\bar\sigma\sigma'}\}. \quad (7)$$

The Keldysh self-energy $\Sigma^<_\sigma(\epsilon) = i\sum_\gamma \Gamma_{\gamma\sigma}(\epsilon)f_\gamma(\epsilon)$ is involved in the Keldysh Green's function. In our system, the wide-band limit approximation is invalid, and the real part of the self-energy $\Sigma^r_\sigma(\epsilon)$ has contributions to the transport.

Substituting the Green's functions given in equations (6) and (7) into current formula (3), we obtain the final expression of spin dependent current explicitly by

$$J^L_{\sigma\sigma} = \frac{1}{h}\sum_{\ell}\int d\epsilon\{T_\sigma(\epsilon,\epsilon)[f_L(\epsilon)-f_R(\epsilon)] + T_\sigma(\epsilon,w_\sigma)\xi^2|\tilde{G}^r_{\ell\bar{\sigma}}(w_\sigma)|^2[f_L(\epsilon)-f_R(w_\sigma)]\}, \quad (8)$$

where $T_\sigma(\epsilon,\tilde{\epsilon})$ is a part of transmission coefficient for electrons tunnelling through the system defined by

$$T_\sigma(\epsilon,\tilde{\epsilon}) = \frac{\Gamma_L(\epsilon)\Gamma_R(\tilde{\epsilon})|\tilde{G}^r_{\ell\sigma}(\epsilon)|^2}{|1-\xi^2\tilde{G}^r_{\ell\sigma}(\epsilon)\tilde{G}^r_{\ell\bar{\sigma}}(w_\sigma)|^2}.$$

The tunnelling current reduces to the Landauer-Büttiker formula as the spin-flip effect is removed by setting $\theta = n\pi$, or by letting $B_0 \to 0$. As the source-drain bias is zero, i.e., $\mu_L - \mu_R = eV = 0$, the charge current disappears, while the spin current is nonzero as $\theta \neq n\pi(n = 0, \pm1, \pm2, \ldots)$. The spin current is induced by the rotating magnetic field $\mathbf{B}(t)$ to form spin flip which is intimately associated with the photon absorption procedure. The spin current also disappears when $\omega \to 0$ even if the spins are polarized as $\theta \neq n\pi$. On the contrary, as the source-drain bias $\mu_L - \mu_R = eV \neq 0$, the spin current and the charge current are both nonzero as $\theta \neq n\pi(n = 0, \pm1, \pm2, \ldots)$, $\omega \neq 0$, and $B_0 \neq 0$. As $\theta = n\pi$, the spin current disappears, and the charge current is the unique tunnelling current. For this case, the Zeeman field only splits the energy spectrum to form non-degenerate system, and the Zeeman splitting is symmetric about magnetic field $B_0$.

## 3 Numerical calculation

We perform the numerical calculation of tunnelling current at zero temperature since it provides rich quantum characteristics. The Fermi function becomes the step function $f_\gamma(\epsilon) = 1 - \theta(\epsilon - \mu_\gamma)$, and the tunnelling current formula in equation (8) is reduced to

$$J^L_{\sigma\sigma} = \frac{1}{h}\sum_{\ell}\{\int_0^{eV} T_\sigma(\epsilon,\epsilon)d\epsilon + \int_{\sigma\hbar\omega}^{eV} T_\sigma(\epsilon,w_\sigma)\xi^2|\tilde{G}^r_{\ell\bar{\sigma}}(w_\sigma)|^2 d\epsilon\}, \quad (9)$$

where we have taken $\mu_R$ as the reference of energy measurement by setting $\mu_R = 0$. The spin and charge currents are nonzero as $eV \neq 0$. For this situation, the spin and charge currents coexist in the same nano-device, and the spin-flip effect contributes to the two currents obviously. Since the source-drain bias is nonzero, electrons are excited to tunnel in the multi-channels of CN leads. This indicates that the structures of CN leads contribute significant effects to tunnelling current. We can employ the characteristics of the two currents by adjusting source-drain bias. When the source-drain bias voltage is zero, the tunnelling current formula in equation (9) is directly reduced to

$$J^L_{\sigma\sigma} = \frac{1}{h}\sum_{\ell}\int_{\sigma\hbar\omega}^{0} T_\sigma(\epsilon,w_\sigma)\xi^2|\tilde{G}^r_{\ell\bar{\sigma}}(w_\sigma)|^2 d\epsilon. \quad (10)$$

The charge current is zero, while the spin current is nonzero, i.e., $I_c = 0$, and $I_s \neq 0$, which is discussed in reference [8] on considering the system composed of a central regime and two normal metal leads. For this special situation, there exists only spin current, and one can use such devices to generate pure spin current. In the numerical calculations, energy is scaled by $\gamma = 10^{-3}\gamma_0 = 3.033$ meV, spin current is scaled by $I_{s0} = \gamma/(4\pi)$, and charge current is scaled by $I_{c0} = e\gamma/h$. The derivatives of spin-flip currents in our system are scaled by $G_{c0} = e\mu_B\gamma/h$, $G_{s0} = \mu_B\gamma/(4\pi)$, and $G_{\omega 0} = \gamma/4$. For the weakly coupled system, the coupling strengths of CN leads with the central QD are chosen as $|R_L| = |R_R| = 6.0$ meV. Usually, the parameters $|R_\gamma|$ and energy levels $E^0_\ell$ should be calculated by first principle approach self-consistently according to the model and engineering. We consider the single level QD by setting $E^0_1 = 0$, which gives the main physical picture for the electrons tunnelling through the system. The multi-level quantum dot only provides multi-resonant structure around the levels of QD $E^0_\ell$ [25]. Further more, the non-zero single level QD gives the energy shifting to form a resonant peak around $E^0_1$, which does not affect the physical properties. The energy of coupled QD is modified, and the self-energy is involved in the energy level for the compound system. The real part of self-energy of leads is determined by the principal value integral, which is zero in wide-band limit by considering the DOS of leads as an energy-independent quantity [27]. However, for our system this term is not zero, and the energy of the coupled QD is modified by

$$\mathrm{Re}\Sigma^r_\sigma(\epsilon) = \sum_\gamma \mid R_\gamma \mid^2 \int_{-\infty}^{+\infty} \frac{1}{\epsilon-\epsilon_1}\rho_{\gamma\sigma}(\epsilon_1)d\epsilon_1.$$

In fact, the real part of the self-energy provides additional discrete energy channels for electrons to tunnel. The self-energy is not related to the external biases as $eV_g$, $eV$, or $\hbar\omega$. This is equivalent to the case that the single-level QD becomes a multi-level QD. The splitting of energy level is related to the DOS of the leads, as well as the coupling strengths.

Figure 1 shows the spin current $I_s$ versus gate voltage $V_g$ for different photon energy $\hbar\omega$ at zero source-drain bias. Two metallic armchair CNs (9,9) are chosen to form a symmetric coupled system. The photon energy is chosen to be located in the order of microwave field regime, where $\hbar\omega = 0.1$ meV corresponds to $2.39 \times 10^{10}$ Hz. As the frequency is low, a single resonant peak emerges at $eV_g = 0$. As the photon energy increases from 0.2 meV to 0.5 meV, the resonant peak is suppressed, and the single peak is split into two major peaks (diagram (a)). As the photon energy changes to 0.6 meV, the maximum of $I_s$ continues to be suppressed, and the split peaks become two small side hills. This means that the regime of tunnelling current

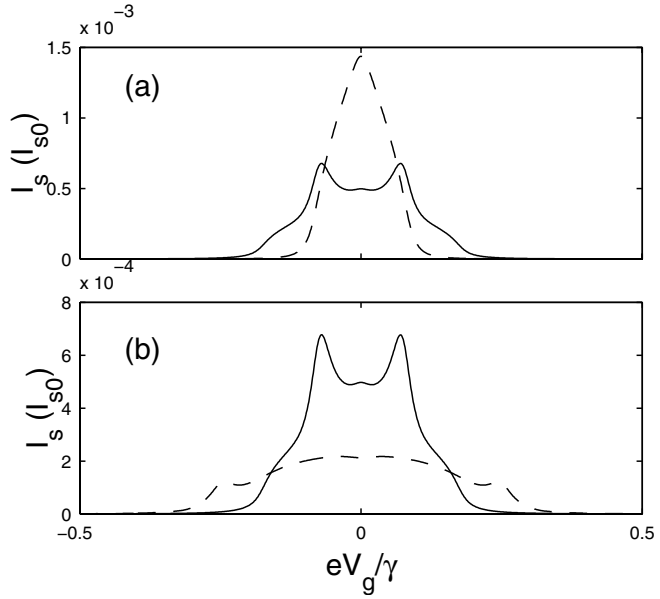


**Fig. 1.** The spin current $I_s$ versus gate voltage $V_g$ with zero source-drain bias for the (9,9)-QD-(9,9) system. The parameters are chosen as $B_0 = 0.5$ T, $\theta = 75°$. The solid curves are associated with $\hbar\omega = 0.5$ meV , while the dashed curves are associated with $\hbar\omega = 0.2$ meV in diagram (a) and $\hbar\omega = 0.6$ meV in diagram (b).

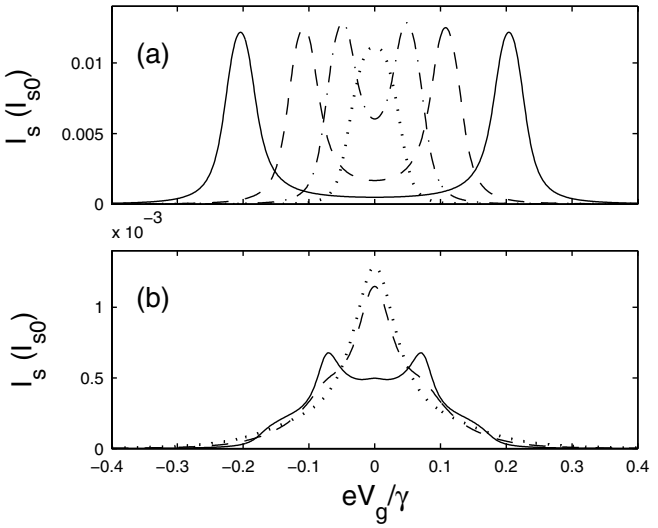


**Fig. 2.** The spin current $I_s$ versus gate voltage $V_g$ with zero source-drain bias for different magnetic fields and CN leads. Diagram (a) is associated with the (9,9)-QD-(9,9) system as $\hbar\omega = 0.1$ meV and $\theta = 75°$. The dotted, dash-dotted, dashed and solid curves correspond to $B_0 = 1.2$ T, 3.0 T, 6.0 T and 11.0 T, respectively. Diagram (b) is related to the systems with different CN leads for $B_0 = 0.5$T, $\hbar\omega = 0.5$ meV and $\theta = 75°$. The solid, dashed and dotted curves correspond to (9,9)-QD-(9,9), (9,9)-QD-(9,0) and (9,0)-QD-(9,0), respectively.

increases with increasing of photon energy, but the magnitude of spin current is suppressed as a compensation. As the photon energy increases, many excited electrons participate in transporting through different channels.

We present the spin current versus gate voltage in Figure 2 to show the variation of spin current with respect to different magnetic fields and CN leads. From diagram (a), one observes that as the magnitude of magnetic field $B_0$ is small, there exists only one resonant peak. As the magnetic field becomes strong enough, the single resonant peak is split to form double resonant peaks, and the peaks are separated completely as $B_0$ becomes stronger. This also manifests the situation that the spin current is adjusted by the gate voltage $V_g$ obviously. Similar result can be obtained for different $\theta$. In diagram (b), we display spin current for the system coupled with different metallic CN leads. The spin current of the system (9,9)-QD-(9,9) possesses two symmetric peaks with respect to the gate voltage. The two side peaks become two shoulders, and the main resonant peak increases obviously by replacing the CN leads to form (9,9)-QD-(9,0) and (9,0)-QD-(9,0) systems. This indicates that the pure spin current is sensitively dependent on the CN leads, and the structure of CN leads makes important contribution to the pure spin current in the absence of source-drain bias.

Figure 3 shows the derivatives of spin and charge currents $dI_s/dB_0$, $dI_c/dB_0$ versus the Zeeman energy in the presence of source-drain bias. The derivative of tunnelling current versus Zeeman field can tell us the information of detailed variation of current with the Zeeman energy. The different curves represent different CN-QD-CN systems. One observes that the derivative is strongly dependent on

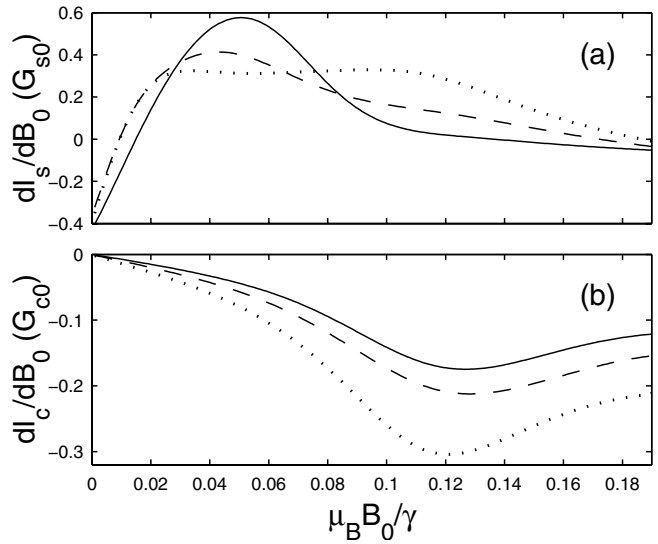


**Fig. 3.** The derivative of spin and charge currents $dI_s/dB_0$, $dI_c/dB_0$ versus the Zeeman energy $\mu_B B_0$ with nonzero source-drain bias. The parameters are chosen as $\hbar\omega = 0.5$ meV, $\theta = 75°$, $V_g = 0$ and $eV = 0.6$ meV. The solid, dashed and dotted curves correspond to the (9,9)-QD-(9,9), (9,9)-QD-(9,0) and (9,0)-QD-(9,0) systems, respectively.

the structure of CN leads and the Zeeman energy. In diagram (a), the derivative $dI_s/dB_0$ increases rapidly from negative value to a maximum value, and then decays as the Zeeman energy increases for (9,9)-QD-(9,9) system. The derivative property of the (9,9)-QD-(9,0) system is similar to that of the (9,9)-QD-(9,9) system, but possesses different magnitude and position of maximum value. The

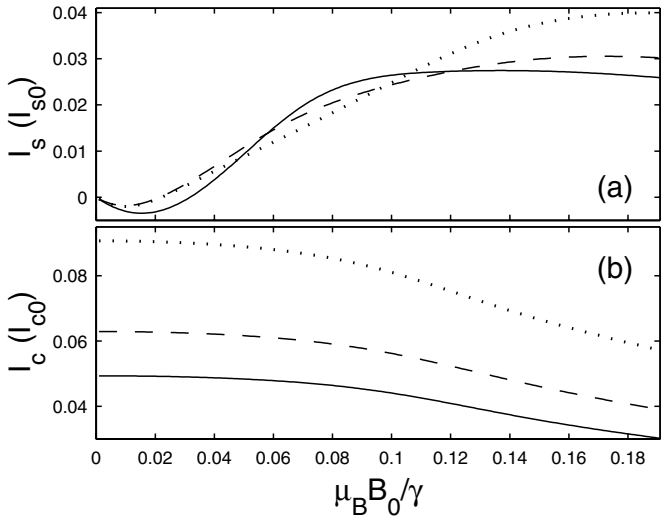


**Fig. 4.** The spin current $I_s$ and charge current $I_c$ versus the Zeeman energy at nonzero source-drain bias. The parameters are chosen as $\hbar\omega = 0.5$ meV, $\theta = 75°$, $V_g = 0$ and $eV = 0.6$ meV. The solid, dashed and dotted curves correspond to the (9,9)-QD-(9,9), (9,9)-QD-(9,0) and (9,0)-QD-(9,0) systems, respectively.

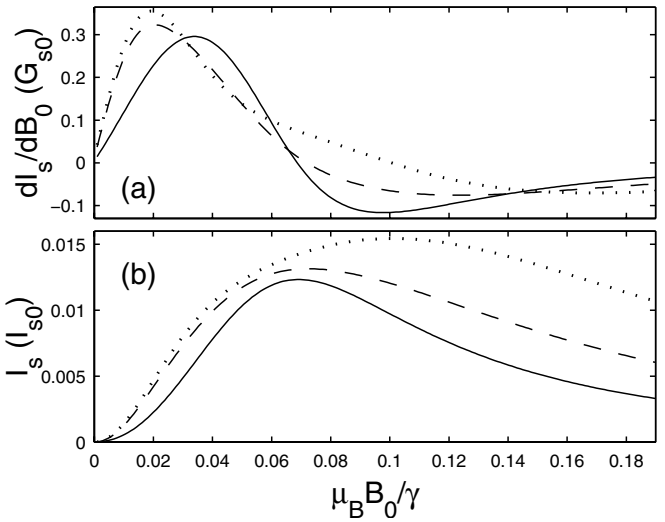


**Fig. 5.** The derivative of spin current $dI_s/dB_0$ and the spin current $I_s$ versus the Zeeman energy $\mu_B B_0$ with zero source-drain bias. The parameters are chosen as $\hbar\omega = 0.5$ meV, $\theta = 75°$ and $V_g = 0$. The solid, dashed and dotted curves correspond to the (9,9)-QD-(9,9), (9,9)-QD-(9,0) and (9,0)-QD-(9,0) systems, respectively.

derivative feature of the (9,0)-QD-(9,0) system is quite different from the two others (dotted curve). There are no obvious peaks compared with the former systems, but it possesses a wide plateau. The fact for a derivative curve changing its sign from negative to positive signifies that there exists a valley at $dI_s/dB_0 = 0$. As the Zeeman energy is much large, $\mu_B B_0 \gg \gamma_0$, the derivative reaches zero. This indicates that the spin current reaches its saturate value. In diagram (b), the derivative of charge current $dI_c/dB_0$ versus the Zeeman energy possesses similar behaviors in the three systems with a negative valley at about $\mu_B B_0 = 0.12\gamma$. The depths of valleys are different from each other among the three systems. The valley of (9,0)-QD-(9,0) system is the deepest one. The negative of derivative charge current tells that the charge current decreases as the Zeeman energy increases. The valley of the derivative signifies that there exists a saddle point at about $\mu_B B_0 = 0.12\gamma$ in the charge current.

The spin current $I_s$ and charge current $I_c$ versus Zeeman energy $\mu_B B_0$ in the presence of source-drain bias are displayed in Figure 4. The parameters are chosen corresponding to the ones in Figure 3. The spin current declines as the Zeeman energy increases, and then it increases to its saturate value. The solid curve (for (9,9)-QD-(9,9)) shows obvious difference from the other two curves as $\mu_B B_0 < 0.12\gamma$. The saturate values are also different from different systems. The nonlinear current changes from zero to its minimum value (negative), and then to its positive saturate value. However, the behavior of charge current is simple for possessing a maximum value at $\mu_B B_0 = 0$. The charge current declines monotonically as the Zeeman energy increases. The magnitudes of charge currents are different for the systems with different CN leads. One observes that the system (9,0)-QD-(9,0) can provide larger charge and spin currents, while the system (9,9)-QD-(9,9) contains rich tunnelling properties compared with the other two systems.

Figure 5 shows the spin current and the derivative of spin current $dI_s/dB_0$ at zero source-drain bias versus the Zeeman energy $\mu_B B_0$. The charge current disappears, and the spin current is determined by equation (10) for $eV = 0$. When the Zeeman energy increases, the derivative of current $dI_s/dB_0$ increases from zero to its maximum value. It declines to its valley (diagram (a)), and then the derivative of spin current increases again to reach its saturate value as $\mu_B B_0 \gg \gamma$. The behaviors of characteristics appear distinct difference among the different systems. The peak-valley behavior in the derivative of spin current indicates nonlinear and non-monotonic characteristics of spin current versus the Zeeman energy, (depicted in diagram (b)). We observe that the $I_s - \mu_B B_0$ characteristics are much different as $eV = 0$ and $eV \neq 0$ shown in Figures 4 and 5. The maximum value of spin current is also different. This indicates that the source-drain bias affects the spin current due to the injection of excited electrons through multi-channels in the CN leads.

The spin current $I_s$ and charge current $I_c$ versus source-drain bias $eV$ are displayed in Figure 6. The spin current resonates at $eV = 0$, and it exhibits quantum steps on the two sides symmetrically. The spin current changes sign as the absolute value of the source-drain bias $|eV|$ increases shown in diagram (a). The magnitude of spin current is shifted in the three different systems, and the positive values are located around the resonant point $eV = 0$. In diagram (b), we see that the charge current disappears at $eV = 0$, and it increases nonlinearly as $eV$

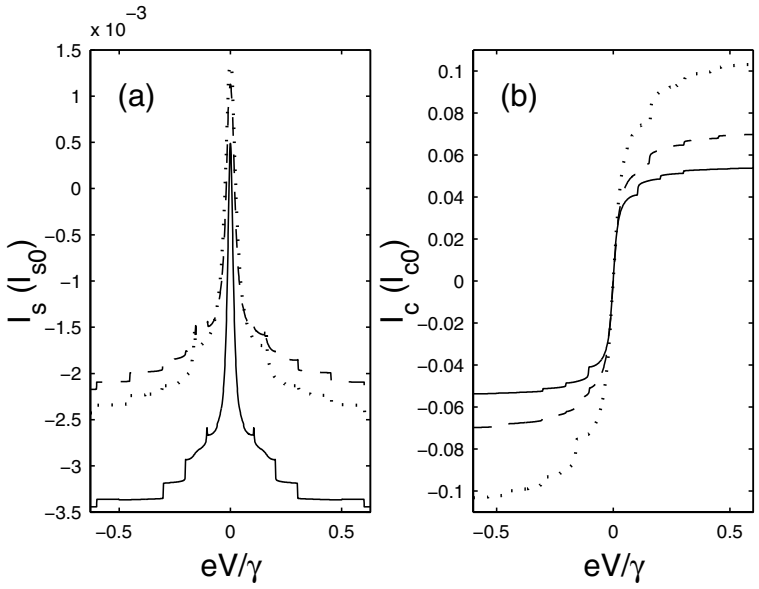


**Fig. 6.** The spin and charge current-voltage characteristics $I_s - V$ and $I_c - V$. The parameters are chosen as $B_0 = 0.5$ T, $\hbar\omega = 0.5$ meV, $\theta = 75^\circ$ and $V_g = 0$. The solid, dashed and dotted curves correspond to the (9,9)-QD-(9,9), (9,9)-QD-(9,0) and (9,0)-QD-(9,0) systems, respectively.

increases. Obvious steps in the I-V characteristics of the charge current are observed. The quantum steps are contributed by the two facts: one is the photon absorption and emission procedure caused by the rotating magnetic field, and the other is induced by the quantum nature of CN leads. The magnitude of charge current reaches different saturate values as $eV \gg \gamma$ for the systems with different CN leads. The spin-flip effect is also involved in the charge current.

Figure 7 displays the spin current $I_s$ and charge current $I_c$ versus gate voltage $V_g$ biased by the source-drain voltage as $eV = 0.6$ meV. The spin current appears different resonant structure compared with the situation as $eV = 0$ shown in Figures 1 and 2. The asymmetric peak and valley characteristics indicate the deviation of Breit-Wigner resonance, but the tunnelling is related to the Fano resonant tunnelling. The positive peak and negative valley are resulted from the competition of the two components of current in equation (9) when $eV \neq 0$. The systems with different CN leads possess different heights of peaks and depths of valleys. We present the charge current versus gate voltage in diagram (b) to shown resonance of charge current. The resonant peaks are asymmetric, and they are also deviated from the usual Breit-Wigner resonances. This asymmetric effect comes from the spin-flip effect and the excited tunnelling in multi-channels of CN leads when $eV \neq 0$. The tunnelling electrons are scattered by the rotating field, and the unbalanced spin reflections cause the asymmetric spin-dependent mesoscopic transport. The magnitudes and shapes of tunnelling charge currents are intimately related to the structures of CN leads.

The spin current is in fact generated from the applied rotating magnetic field. It also strongly associated with the concrete quantum system. We exhibit the spin current

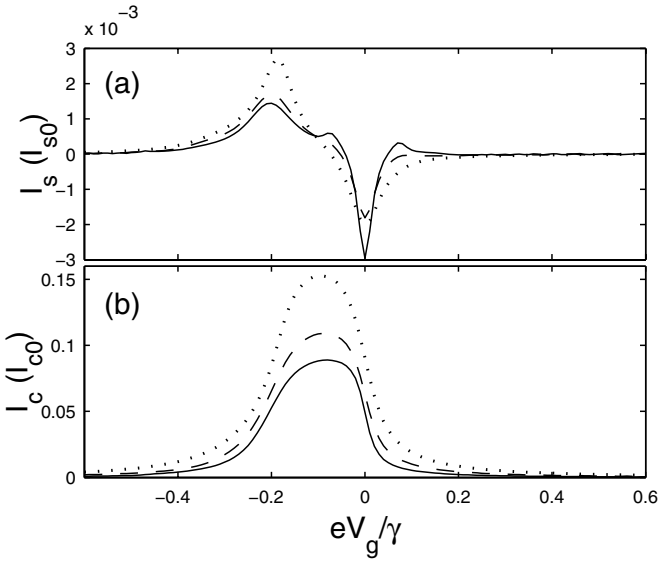


**Fig. 7.** The spin current $I_s$ and the charge current $I_c$ versus gate voltage $V_g$ with nonzero source-drain bias. The parameters are chosen as $B_0 = 0.5$ T, $\hbar\omega = 0.5$ meV, $\theta = 75^\circ$ and $eV = 0.6$ meV. The solid, dashed and dotted curves correspond to the (9,9)-QD-(9,9), (9,9)-QD-(9,0) and (9,0)-QD-(9,0) systems, respectively.

$I_s$ versus photon energy of the rotating magnetic field $\hbar\omega$ in Figure 8 for the two cases as $eV = 0.6$ meV in (a), and $eV = 0$ in (b). Multi-resonant peaks of spin current appear versus the photon energy $\hbar\omega$, and the heights of resonant peaks decline as the magnitude of photon energy increases. These multi-resonant spin current structures are associated with the CN quantum wires. The DOS of a CN lead makes important contribution to the

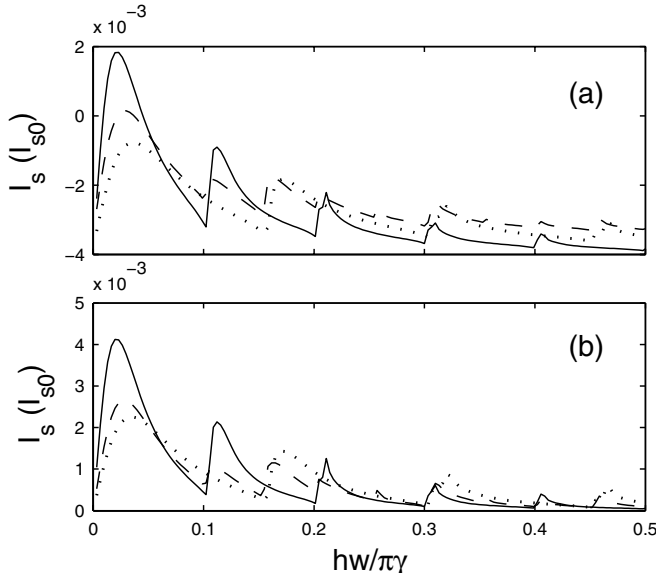


**Fig. 8.** The spin current $I_s$ versus photon energy $\hbar\omega$. The parameters are chosen as $B_0 = 0.5$ T, $\theta = 75^\circ$ and $V_g = 0$. Diagrams (a) and (b) are spin currents at $eV = 0.6$ meV, and $eV = 0$, respectively. The solid, dashed and dotted curves correspond to the (9,9)-QD-(9,9), (9,9)-QD-(9,0) and (9,0)-QD-(9,0) systems, respectively.

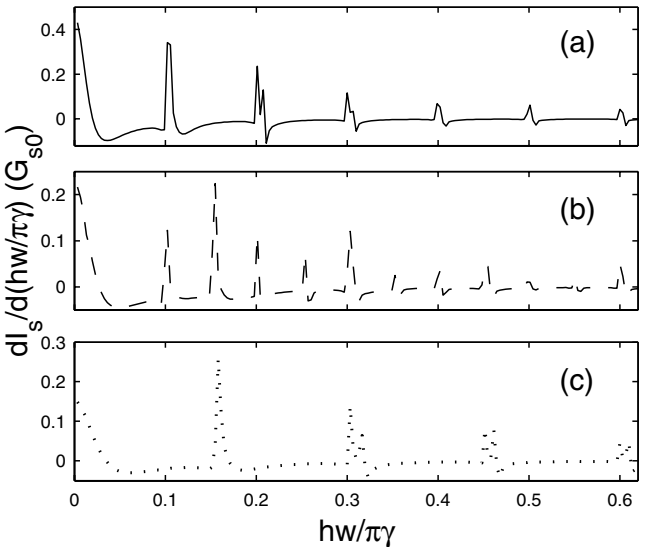


**Fig. 9.** The derivative of spin current $dI_s/d\hbar\omega$ versus photon energy $\hbar\omega$. The parameters are chosen as $B_0 = 0.5$ T, $\theta = 75^\circ$ and $V_g = 0$. Diagrams (a), (b) and (c) are derivatives of spin current at $eV = 0.6$ meV. The solid, dashed and dotted curves correspond to the (9,9)-QD-(9,9), (9,9)-QD-(9,0) and (9,0)-QD-(9,0) systems, respectively.

spin current. Different CN systems possess different resonant tunnelling structures, which can be seen from the different curves. The applied source-drain bias voltage induces the effect to shift spin current down to a negative value. As the bias voltage $V$ is removed, the spin current exhibits similar resonant structure as the case where $V \neq 0$, but the magnitude of the current moves to the positive regime. This also signifies that the CN structures are involved in the mesoscopic transport in the pure spin current. The single peak effect has been discussed for the system as the QD is coupled to normal leads in references [8] and [12]. We present the derivative of spin current $dI_s/d\hbar\omega$ when $eV = 0.6$ meV in Figure 9a, b and c for different CNs coupled systems, respectively. The derivative of spin current displays explicit resonant structures for different CNs coupled systems. The photon absorption and emission procedure cause novel channels in QD, and the matching-mismatching of channels in the CN leads with QD determines the tunnelling properties.

## 4 Summary and discussion

We have investigated mesoscopic transport through the systems consisted of a central QD and two SWCN leads in the presence of a rotating magnetic field. The calculations of charge and spin current components show the intimate relation with SWCN leads. Specific DOS structures of concrete SWCN leads dominate the detailed spin and charge transport significantly. The Zeeman effect is important when the magnitude of magnetic field $B_0$ is strong enough. The spin-flip effect is induced by the rotating magnetic field, and the tunnelling current is sensitively related to the spin-flip effect. The current characteristics are much different for the system when $eV = 0$ and $eV \neq 0$. The source-drain bias can modify the spin current considerably due to injecting excited electrons through multichannels of CN leads. The asymmetric peak and valley of spin current versus gate voltage characteristics exhibit Fano resonance. This asymmetric effect comes from the spin-flip effect and the unbalanced spin reflections. Multiresonant peaks of spin current versus the photon energy $\hbar\omega$ reflects the structure of CN quantum wires and resonant photon absorption and emission effect. The photon absorption and emission procedure cause novel channels in QD, and the matching-mismatching of channels in the CN leads and QD results in the multi-resonant spin current structure by tuning the frequency of rotating field. We can employ this kind of CN-FET-CN devices to supply multi-resonant charge and spin current by controlling the external parameters $V$, $B_0$, $V_g$, and $\omega$.

This work was supported by the National Natural Science Foundation of China under the Grant No. 10375007, and by the Fundamental Research Foundation of Beijing Institute of Technology.

## References

1. G.A. Prinz, Science **282**, 1660 (1998)
2. S. Datta, B. Das, Appl. Phys. Lett. **56**, 665 (1990)
3. P. Recher, E.V. Sukhorukov, D. Loss, Phys. Rev. Lett. **85**, 1962 (2000)

4. T. Koga, J. Nitta, H. Takayanagi, S. Datta, Phys. Rev. Lett. **88**, 126601 (2002)
5. A. Brataas, Y. Tserkovnyak, G.E.W. Bauer, B. Halperin, Phys. Rev. B **66**, 060404 (2002)
6. Q.F. Sun, H. Guo, J. Wang, Phys. Rev. Lett. **90**, 258301 (2003)
7. W. Long, Q. F. Sun, H. Guo, J. Wang, Appl. Phys. Lett. **83**, 1397 (2003)
8. B. Wang, J. Wang, H. Guo, Phys. Rev. B **67**, 092408 (2003); P. Zhang, Q.K. Xie, X.C. Xie, Phys. Rev. Lett. **91**, 196602 (2003)
9. J. König, M.C. Bonsager, A.H. MacDonald, Phys. Rev. Lett. **87**, 187202 (2001)
10. F. Meier, D. Loss, Phys. Rev. Lett. **90**, 167204 (2003)
11. S.A. Wolf et al., Science **294**, 1488 (2001); R. Fiederling et al., Nature (London) **402**, 787 (1999); Y. Ohno et al., Nature (London) **402**, 790 (1999)
12. H.K. Zhao, J. Wang, Eur. Phys. J. B **44**, 93 (2005); H.K. Zhao, Q. Wang, Phys. Lett. A, **338**, 425 (2005)
13. S. Iijima, Nature (London) **354**, 56 (1991); D.S. Bethune et al., Nature (London) **363**, 605 (1993); S.J. Tans et al., Nature (London) **386**, 474 (1997)
14. K. Tsukagoshi et al., Nature (London) **401**, 572 (1999)
15. S. Heinze et al., Phys. Rev. Lett. **89**, 106801 (2002); A.A. Odintsov, Phys. Rev. Lett. **85**, 150 (2000)
16. Z. Yao , H.W.Ch. Postma, L. Balents, C. Dekker, Nature (London) **402**, 273(1999)
17. S.J. Tans, A.R.M. Verschueren, C. Dekker, Nature (London) **393**, 49 (1998); R. Martel et al., Appl. Phys. Lett. **73**, 2447 (1998)
18. R. Tamura, Phys. Rev. B **67**, 121408 (2003)
19. X. Blase, L.X. Benedict, E.L. Shirley, S.G. Louie, Phys. Rev. Lett. **72**, 1878 (1994); Yu.A. Krotov, D.H. Lee, S.G. Louie, Phys. Rev. Lett. **78**, 4245 (1997)
20. J. Taylor, H. Guo, J. Wang, Phys. Rev. B **63**, 245407 (2001)
21. R. Egger, A.O. Gogolin, Phys. Rev. Lett. **79**, 5082 (1997); R. Egger, Phys. Rev. Lett. **83**, 5547 (1999)
22. C.L. Kane, L. Balents, M.P.A. Fisher, Phys. Rev. Lett. **79**, 5086 (1997)
23. M. Buongiorno Nardelli, Phys. Rev. B **60**, 7828 (1999); D. Orlikowski et al., Phys. Rev. B **63**, 155412 (2001)
24. R. Saito, G. Dresselhaus, M.S. Dresselhaus, *Physical Properties of Carbon Nanotubes* (Imperial College Press, London, 1998)
25. L.N. Zhao, H.K. Zhao, Phys. Lett. A **325**, 156 (2004); L.N. Zhao, H.K. Zhao, Int. J. Mod. Phys. B **18**, 2071 (2004)
26. L.N. Zhao, H.K. Zhao, Eur. Phys. J. B, **42**, 285 (2004)
27. A.P. Jauho, N.S. Wingreen, Y. Meir, Phys. Rev. B **50**, 5528 (1994)
28. Q.F. Sun, J. Wang, T.H. Lin, Phys. Rev. B **59**, 3831 (1999)
29. H.K. Zhao, Z. Phys. B **102**, 415(1997); H.K. Zhao, G.V. Gehlen, Phys. Rev. B **58**, 13660 (1998); H.K. Zhao, Phys. Rev. B **63**, 205327 (2001)